The chaotic instability of a slowly spinning asymmetric top

G.H.M. van der Heijden* & J.M.T. Thompson*

May 31, 2000

Abstract

We study how a top spinning in an unstable upright state can fall down in a near-homoclinic fashion, i.e., by repeatedly falling down and coming up again. A symmetric top shows regular behaviour but an asymmetric top can behave chaotically with infinitely many homoclinic orbits available. These orbits could be utilised in toppling and recovery manoeuvres of spinning bodies by applying subtle control techniques.

1 Introduction

In previous work we studied the spatial complexity of twisted elastic rods subject to end loading, focussing on localised solutions described by homoclinic orbits of the underlying equilibrium equations (see, e.g., [7, 8]). It is well-known that there is a close analogy between the equations for a twisted rod and those for a spinning top [12, 1]. In this paper we investigate the implications of our previous work on twisted (anisotropic) rods for the behaviour of spinning (asymmetric) tops.

Consider a top that is spinning in an upright state at an angular velocity such that, according to standard bifurcation theory, the top is in a state of unstable relative equilibrium. Given an infinitesimal perturbation it will fall away from the upright configuration. In the absence of dissipation, it will however return, again and again, very close to the upright configuration. In technical terms, its motion will lie very close to a homoclinic orbit that, as time passes from minus infinity to plus infinity, departs from the upright state and returns to it. For a top spinning about an axis of symmetry, the repeated returns will be regular and predictable. However, for a non-symmetric top there are an infinite number of different homoclinic orbits, implying that the repeated returns are chaotic and unpredictable. We use homoclinic path-following techniques to explore the structure of these homoclinic orbits, and illustrate the physical motions involved.

This short paper is organised as follows. In Section 2 the formulation of the spinning top problem is given. The integrable cases are reviewed and a linear stability analysis is presented with the aid of the inertia triangle. Section 3 then discusses the multitude of possible

*Centre for Nonlinear Dynamics, University College London, Gower Street, London WC1E 6BT, UK. E-mail address: g.heijden@ucl.ac.uk, fax: (+44) (0)20 7380 0986.

homoclinic motions and presents some continuation results. The paper closes, in Section 4, with a discussion of the results.

2 The equations for a spinning top

The equation governing the motion of a heavy rigid body about a fixed point is given by (see, e.g., [6])

$$\boldsymbol{m}' = Mg\boldsymbol{k} \times \boldsymbol{c}. \tag{1}$$

Here $\boldsymbol{m}$ is the angular momentum of the rigid body about the fixed point, M is the mass, g is the acceleration due to gravity, $\boldsymbol{k}$ is the vertical basis vector, and $\boldsymbol{c}$ is the vector from the fixed point to the centre of mass of the body. The prime denotes the derivative with respect to time t. Eq. (1) can be rewritten in terms of components with respect to an orthonormal frame that is fixed in the body and which is rotating about the fixed point with instantaneous angular velocity $\boldsymbol{\omega}$:

$$m' = m \times \omega + Mgk \times c, \qquad k' = k \times \omega, \tag{2}$$

where the second equation describes the rotation of the constant vector $\boldsymbol{k}$ as seen from the moving frame. Note that m, k, c and ω denote triples of co-ordinates with respect to the moving frame, while $\boldsymbol{m}$, $\boldsymbol{k}$, $\boldsymbol{c}$ and $\boldsymbol{\omega}$ denote vectors in the fixed inertial frame. Of course, m and ω are related through

$$m = \boldsymbol{I}\omega,$$

where $\boldsymbol{I}$ denotes the inertia tensor of the rigid body about the fixed point. Without loss of generality we shall assume that the body frame has been chosen to coincide with the principal axes of inertia (which go through the pivot point). Thus we can write

$$\boldsymbol{I} = \mathrm{diag}(I_1, I_2, I_3).$$

If the length and time scales

$$|\boldsymbol{c}| \qquad \text{and} \qquad \sqrt{\frac{I}{Mg|\boldsymbol{c}|}} \tag{3}$$

are introduced, in which $I := I_1 + I_2 + I_3$, then the equations (2) can be written out in components as follows:

$$\begin{aligned}
\dot{x}_1 &= x_6x_2 - x_5x_3,\\
\dot{x}_2 &= x_4x_3 - x_6x_1,\\
\dot{x}_3 &= x_5x_1 - x_4x_2,\\
\dot{x}_4 &= \left[(i_2 - i_3)x_5x_6 + c_3x_2 - c_2x_3\right]/i_1,\\
\dot{x}_5 &= \left[(i_3 - i_1)x_4x_6 + c_1x_3 - c_3x_1\right]/i_2,\\
\dot{x}_6 &= \left[(i_1 - i_2)x_4x_5 + c_2x_1 - c_1x_2\right]/i_3,
\end{aligned} \tag{4}$$

where now $c_1^2+c_2^2+c_3^2 = 1$, $i_1+i_2+i_3 = 1$, $i_l = I_l/I$ $(l = 1, 2, 3)$, $k = (x_1, x_2, x_3)$, $\omega = (x_4, x_5, x_6)$, while the overdot denotes the derivative with respect to the rescaled time $\tau = t\sqrt{I/Mg|\boldsymbol{c}|}$. It

follows immediately from their definition (see, e.g., [9]) that the principal inertias (indeed, any triple of inertias) satisfy the inequalities

$$i_k + i_l \geq i_m \qquad (k \neq l \neq m), \tag{5}$$

with the equality holding for planar bodies tumbling about a pivot lying in the plane of the body. At this point we introduce the inertia triangle shown in Fig. 1. It defines all the possible values of the i_k's subject to the constraint $i_1+i_2+i_3 = 1$. The co-ordinates of a point inside the triangle, sometimes called trilinear co-ordinates, are determined by the perpendicular distances to the three sides, as illustrated in Fig. 1 (top left). The inequalities in (5) then define a subtriangle inside which all possible values of the principal inertias are actually situated (Fig. 1 (bottom left)).

System (4) has the following two 'trivial' (geometric) first integrals:

$$x_1^2 + x_2^2 + x_3^2 \qquad \text{(unit vector)}, \tag{6}$$

$$i_1 x_1 x_4 + i_2 x_2 x_5 + i_3 x_3 x_6 \quad \text{(angular momentum about } \boldsymbol{k}\text{)}. \tag{7}$$

They can be used to reduce the six-dimensional system (4) globally to a two-degrees-of-freedom canonical Hamiltonian system (see [16], where this is performed for twisted rods), but that form of the equations becomes awkward in numerical computations so we shall not use it here. In addition, (4) has the energy integral

$$(i_1 x_4^2 + i_2 x_5^2 + i_3 x_6^2)/2 + c_1 x_1 + c_2 x_2 + c_3 x_3 \quad \text{(total energy)}. \tag{8}$$

The following special cases have additional first integrals and are completely integrable:

1. Lagrange top: the centre of mass lies on one of the principal axes, and the moments of inertia about the other two axes are equal, e.g., $c = (0, 0, 1)$, $i_1 = i_2 = (1 - i_3)/2$. Additional integral: x_6, angular momentum about the symmetry axis.

2. Kovalevskaya top: two of the principal moments of inertia are equal and twice the third one, and the centre of mass lies in the plane corresponding to the two equal moments of inertia, e.g., $c = (0, 0, 1)$, $i_1 = i_3 = 2i_2 = 2/5$. Additional integral: $(x_4^2 - x_6^2 + (-c_1 x_1 + c_3 x_3)/i_2)^2 + (2x_4 x_6 - (c_3 x_1 + c_1 x_3)/i_2)^2$.

3. Goryachev-Chaplygin top: two of the principal moments of inertia are equal and four times the third one, and the centre of mass lies in the plane corresponding to the two equal moments of inertia, e.g., $c = (0, 0, 1)$, $i_1 = i_3 = 4i_2 = 4/9$. Additional integral: $x_5(x_4^2 + x_6^2) - x_2(c_1 x_4 + c_3 x_6)/i_2$. This extra integral is only conserved at zero angular momentum, i.e., if, in addition, we have $i_1 x_1 x_4 + i_2 x_2 x_5 + i_3 x_3 x_6 = 0$.

To this list could be added the case of a free rigid body (gyroscope), except that its defining condition, $\boldsymbol{c} = \boldsymbol{0}$, is incompatible with the scaling used in deriving (4), which makes $\boldsymbol{c}$ into a unit vector. However, c can be set to zero in (2), in which case one obtains the Euler equations, which are again integrable [6]. These four cases exhaust all the integrable cases of (4).

From now on we shall consider the case $c = (0, 0, 1)$, but with no conditions imposed on the i_k (apart from the normalisation condition $i_1 + i_2 + i_3 = 1$). Thus, (4) is treated as a two-parameter family of equations (a unique set of equations for each point of the subtriangle

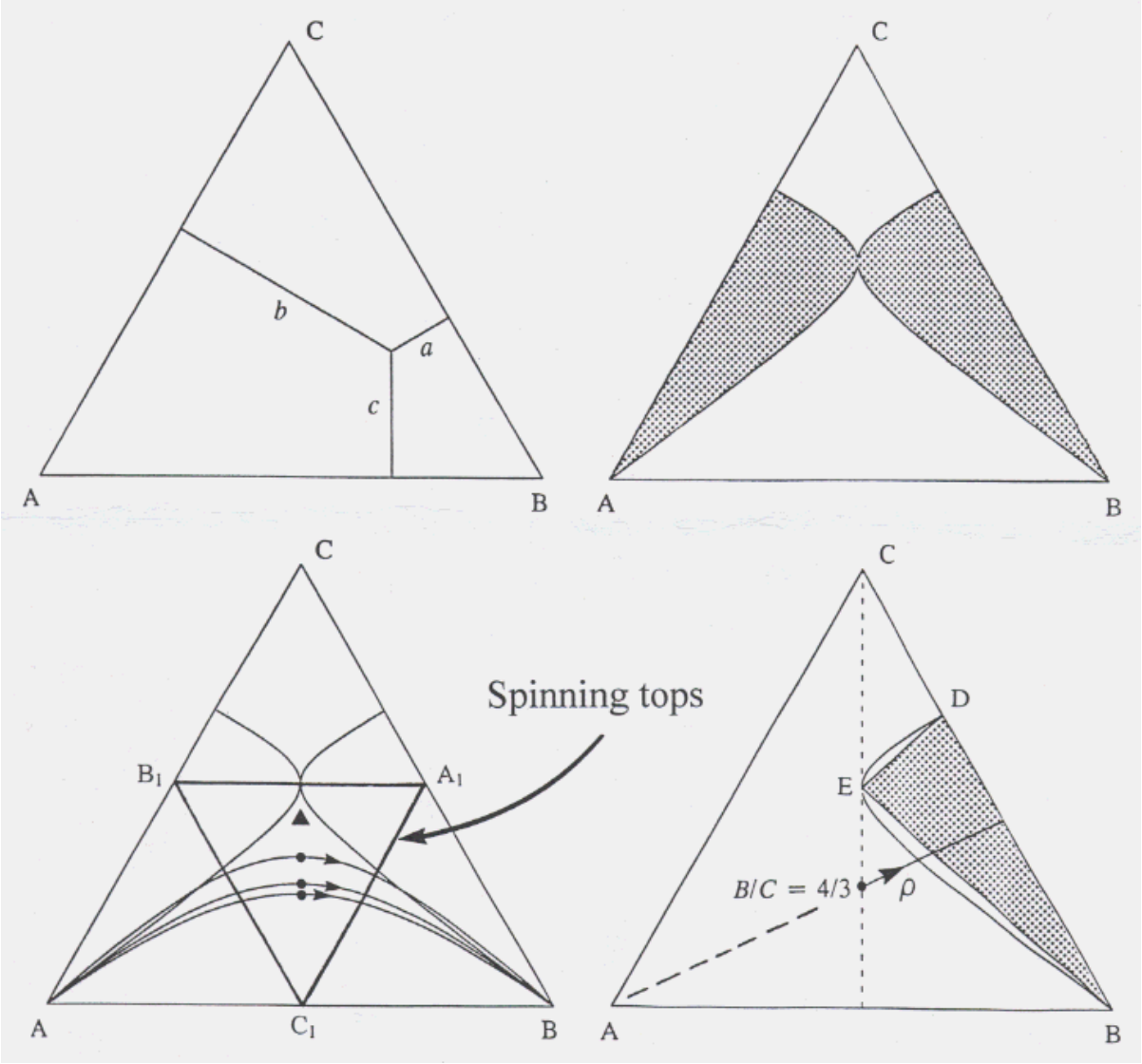

Figure 1: The inertia triangle and its geometry. (Top left) an equilateral triangle of unit height has $a + b + c = 1$. The ratios of the moments of inertia are given by $A : B : C = a : b : c$. (Top right) two symmetrically placed curves of tangencies (where all eigenvalues are zero); they touch at $C = 2B = 2A$. (Bottom left) A top has $a + b > c$, etc. (cf. (5)). Hence all tops lie in the subtriangle $A_1B_1C_1$. Boundary lines of this subtriangle have $a + b = c$ etc., and represent planar bodies. For instance, if $a + b = c$ then $c = 1/2$ and the top lies in the plane through the pivot and normal to $\boldsymbol{k}$. At C_1 the top is a *pole*, at A_1 and B_1 a *perch*. (The curves running from A to B define the stiffnesses for families of solid elliptical rods.) (Bottom right) The shaded zones are zones with no complex eigenvalues at any spin speed ω_0. The lines DE and EB are lines of limit points along the ω_{c1} curves in Fig. 2. The straight line with arrow defines a typical family of asymmetric tops.

in Fig. 1 (bottom left)). It is well-known that the system of equations (4) is then equivalent to that describing the bending and twisting of a linearly elastic inextensible rod held by end forces and twisting moments, and with $\dot{\boldsymbol{r}} = \boldsymbol{c}$, where $\boldsymbol{r}$ describes the centre line of the rod. This is known as Kirchhoff's kinetic analogy [12, 1]. In the rod, the i_k are the bending and torsional stiffnesses, the components of k the shears and the tension, and the components of ω the bending and twisting strains.

With $c = (0, 0, 1)$, (4) is invariant under the two reversing involutions

$$R_1: \quad (x_1, x_2, x_3, x_4, x_5, x_6) \to (-x_1, x_2, x_3, -x_4, x_5, x_6), \quad t \to -t, \tag{9}$$

$$R_2: \quad (x_1, x_2, x_3, x_4, x_5, x_6) \to (x_1, -x_2, x_3, x_4, -x_5, x_6), \quad t \to -t. \tag{10}$$

Together they imply invariance under the reflection symmetry $Z = R_1 R_2 = R_2 R_1$:

$$Z: \quad (x_1, x_2, x_3, x_4, x_5, x_6) \to (-x_1, -x_2, x_3, -x_4, -x_5, x_6). \tag{11}$$

These symmetry properties will be important later in determining the number of homoclinic orbits of the system, i.e., the number of ways a slowly spinning upright top can fall down.

The system has the following two-parameter family of fixed points:

$$\bar{x} = (0, 0, k_0, 0, 0, \omega_0). \tag{12}$$

Note, however, that we have to choose $k_0 = 1$, because $\boldsymbol{k}$ is a unit vector, while ω_0 is arbitrary. These solutions correspond to tops spinning about the vertical axis with (dimensionless) angular velocity ω_0. The stability of these solutions is determined by the eigenvalues of the fixed points (12), which will depend on the two free parameters of (4) as well as on ω_0. Two of the eigenvalues are zero with eigenvectors $(0, 0, 1, 0, 0, 0)$ and $(0, 0, 0, 0, 0, 1)$, corresponding to the arbitrariness of k_0 (as far as the equations are concerned) and ω_0 in (12). The other four eigenvalues are the roots of the characteristic polynomial of the linearisation of (4) about (12), which in reduced form we can write as

$$P(\lambda) = \lambda^4 + a_2\lambda^2 + a_0, \tag{13}$$

where

$$a_0 = \left[i_1 + (1+\omega_0^2)i_2 + (1-\omega_0^2)i_3\right]\left[(1+\omega_0^2)i_1 + i_2 + (1-\omega_0^2)i_3\right]/(i_1 i_2),$$

$$a_2 = -\left[i_1^2 + i_2^2 - \omega_0^2 i_3^2 + 2(1-\omega_0^2)i_1 i_2 + (1+\omega_0^2)i_1 i_3 + (1+\omega_0^2)i_2 i_3\right]/(i_1 i_2).$$

A codimension-one bifurcation occurs when one of the following conditions is satisfied:

$$\begin{array}{lllll} \text{(i)} & a_2^2 - 4a_0 = 0, & a_2 > 0 & \text{(Hamiltonian-Hopf)}, \\ \text{(ii)} & a_0 = 0, & a_2 < 0 & \text{(Hamiltonian-pitchfork)}, \\ \text{(iii)} & a_0 = 0, & a_2 > 0. & \end{array} \tag{14}$$

In the symmetric case of a Lagrange top ($i_1 = i_2$) a change of stability, through a Hamiltonian-Hopf bifurcation, occurs at a critical angular velocity given by

$$\omega_c = \frac{2\sqrt{i_1}}{i_3}. \tag{15}$$

The upright top is stable at spin speeds higher than ω_c (sleeping top).

In general, the equation $a_0 = 0$ has the solutions

$$\omega_0 = \pm\frac{1}{\sqrt{i_3 - i_1}}, \pm\frac{1}{\sqrt{i_3 - i_2}}. \tag{16}$$

Consequently, there are three different cases:

$$\begin{array}{lll} \text{(i)} & i_3 > i_1, \quad i_3 > i_2 & \text{('oblate')}, \\ \text{(ii)} & i_1 < i_3 < i_2 \quad \text{or} \quad i_2 < i_3 < i_1, & \\ \text{(iii)} & i_3 < i_1, \quad i_3 < i_2 & \text{('prolate')}, \end{array} \tag{17}$$

which can be illustrated by means of the two typical parameter planes in Fig. 2. In each of the diagrams the ratio i_2/i_3 is fixed, and the parameter $\rho := i_2/i_1 - 1$ is varied. Note that ρ is a measure of the asymmetry of the top, taking values between -1 and ∞. A value of ρ in these diagrams fixes a body.

Fig. 2(b) is more complicated than Fig. 2(a) because of an additional line, labelled ω_{c4}, of two zero and two imaginary eigenvalues intersecting the other ω_{c4} line on the vertical axis. This extra line ω_{c4} arises because of the additional solution in (16) if $i_3 > i_2$. It moves up and disappears at infinite ω_0 as $i_2 \to i_3$, leaving a parameter plane as in Fig. 2(a). Note that this extra line ω_{c4} prevents the symmetric top (at $\rho = 0$) from becoming unstable at high spin speed ω_0. In both diagrams there is a vertical asymptote for ω_{c4} at a value of ρ such that $i_3 = i_1$ (cf. (16)).

Also in both diagrams, a line of Hamiltonian-Hopf bifurcations, labelled ω_{c2}, passes through the critical point of the symmetric case given by (15). It runs up to a tangency with a line, labelled ω_{c3}, of Hamiltonian pitchfork bifurcations. At the tangency a_2 changes sign, and the Hopf line continues as a line, labelled ω_{c1}, of double real eigenvalues which reaches a limit point, at $\rho = 2i_2/i_3 - 1$, before it bends back to the origin of the parameter plane. Note that in both diagrams we have a complex quadruple of eigenvalues in the region bounded by ω_{c1} and ω_{c2}. By analogy with our previous work on twisted rods [7] we expect chaotic dynamics in this region of the parameter plane.

Fixing the ratio i_2/i_3 restricts us, in the inertia triangle of Fig. 1, to a straight line coming out of A. If we lift this constraint and introduce a second parameter then we can draw curves of the codimension-two points (tangencies and limit points) in the parameter plane, as is done in Fig. 3, or directly in the inertia triangle, as is done in Fig. 1 (top right and bottom right).

Stable upright tops only exist for parameters in the region of imaginary eigenvalues in Fig. 2. Stability is lost by crossing either the line ω_{c2} or the line ω_{c4}. The natural scenario to consider is to reduce the parameter ω_0 (for instance, friction in a real top will slowly reduce ω_0). In the next section we focus on what happens as the Hamiltonian-Hopf line ω_{c2} is crossed. This includes the case of a symmetric top ($\rho = 0$) and is also the case most relevant for the twisted rod. We note, however, that if $i_2 < i_3$ (Fig. 2(b)) an upright top can also become unstable by crossing the line ω_{c4}, and indeed can be destabilised in this manner by an increase of its spin speed (this 'superfast' top instability is also pointed out in [14]). We will comment further on this possibility in the Discussion.

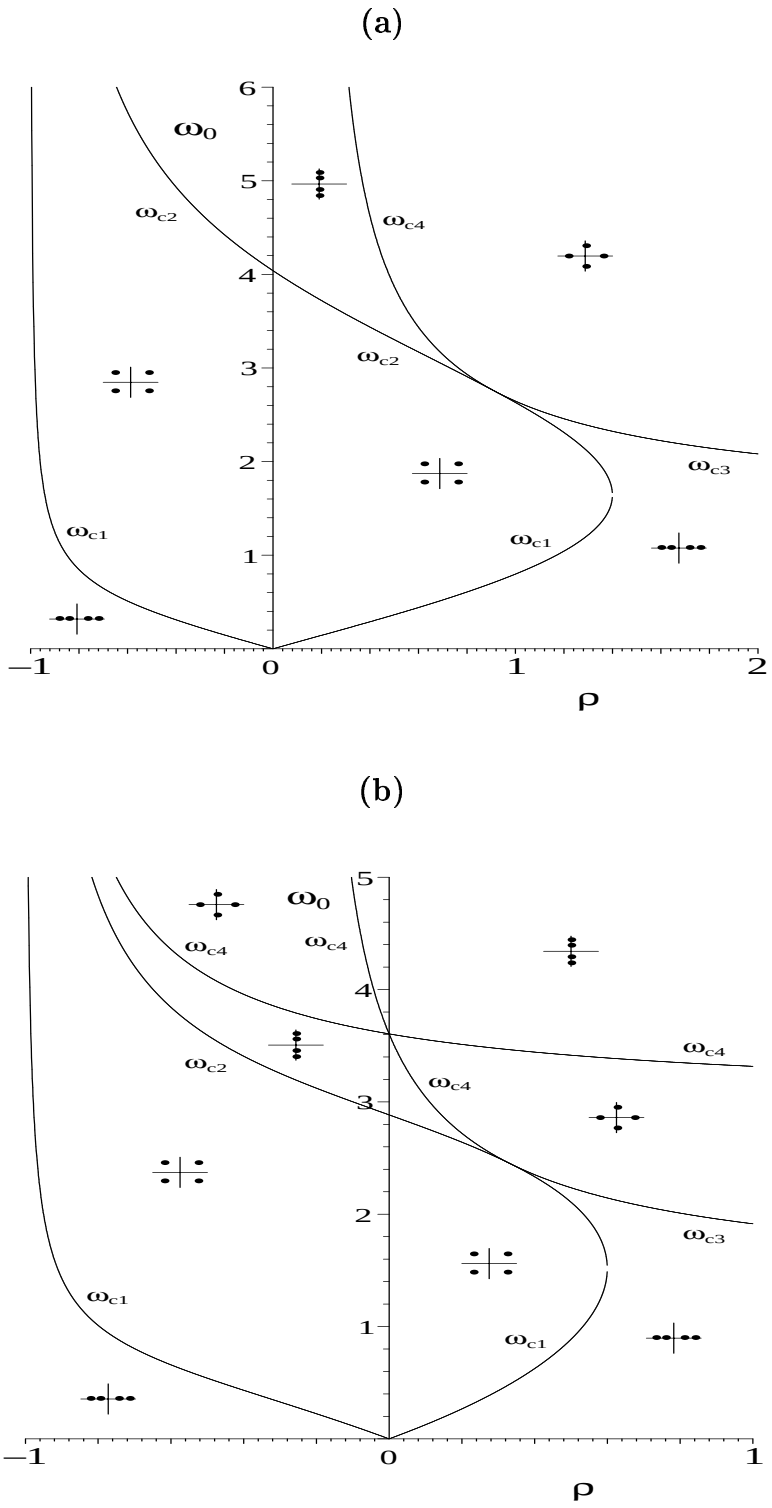

Figure 2: The two cases of the ρ-ω_0 parameter plane with eigenvalue configurations and loci of bifurcation points: (a) $i_2 = (6/5)i_3$, (b) $i_2 = (4/5)i_3$.

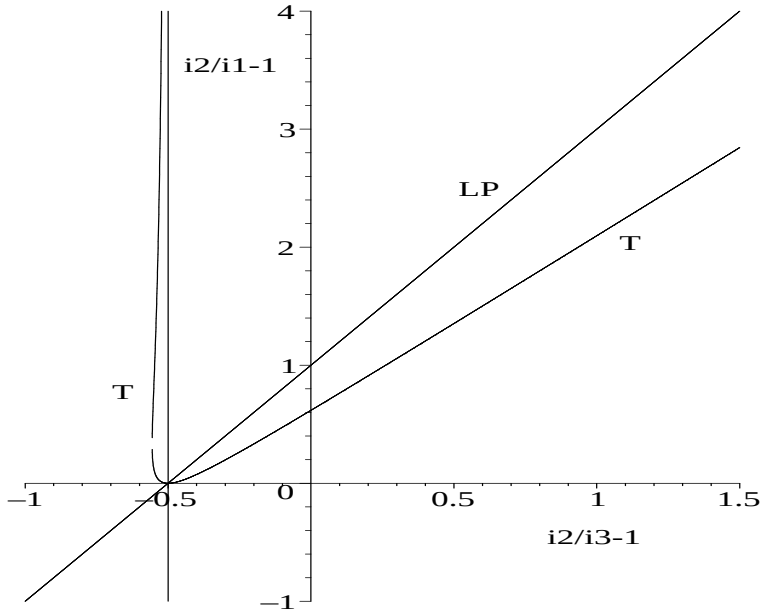

Figure 3: Curves of limit points (LP) and tangencies (T).

3 Falling tops

As already stated, in the symmetric case ($\rho = 0$) the system is completely integrable and we have a symmetric family of homoclinic orbits. By generalising the Melnikov technique to multi-degree-of-freedom Hamiltonian systems, Holmes & Marsden [10] have proved that if i_1/i_3 is sufficiently large and i_2/i_1 sufficiently close to 1 (assuming $i_1 \geq i_2 \geq i_3$), then the invariant manifolds of the trivial saddle points intersect transversely, leading to infinitely many homoclinic orbits and horseshoe-type chaos. In particular this implies that the slightly asymmetric top is non-integrable. In this section we confirm this numerically and show that these analytical results valid asymptotically near $\rho = 0$ actually remain valid well away from the symmetric case.

In fact, we find that the family of homoclinic orbits present in the symmetric case breaks up into four primary homoclinic orbits: a Z-symmetric pair of R_1-reversible homoclinic orbits and a Z-symmetric pair of R_2-reversible homoclinic orbits. Together they represent two physically distinct motions for the top, as illustrated in Fig. 4 for the parameter values $\rho = 0.2$, $\omega_0 = 3$, taken in the region of the parameter plane where we have complex eigenvalues. The existence of these four homoclinic orbits is consistent with the work of Iooss & Pérouème [11] on Hamiltonian-Hopf bifurcations which shows that under some conditions symmetric pairs of homoclinic orbits exist near such a bifurcation (see also [8] where one of these conditions, a normal form sign condition, is verified explicitly). The solutions were computed with the shooting method explained in [7]. The right diagrams in Fig. 4 show the orbits traced out by the top's centre of mass as seen by an inertial observer looking down onto the pivot point.

The primary (single-pulse) homoclinic orbits are numerically found to exist in the entire region of complex eigenvalues in Fig. 2. Since our system is Hamiltonian and reversible, and essentially 4-dimensional, a result by Devaney [5] tells us that we should expect to find, in

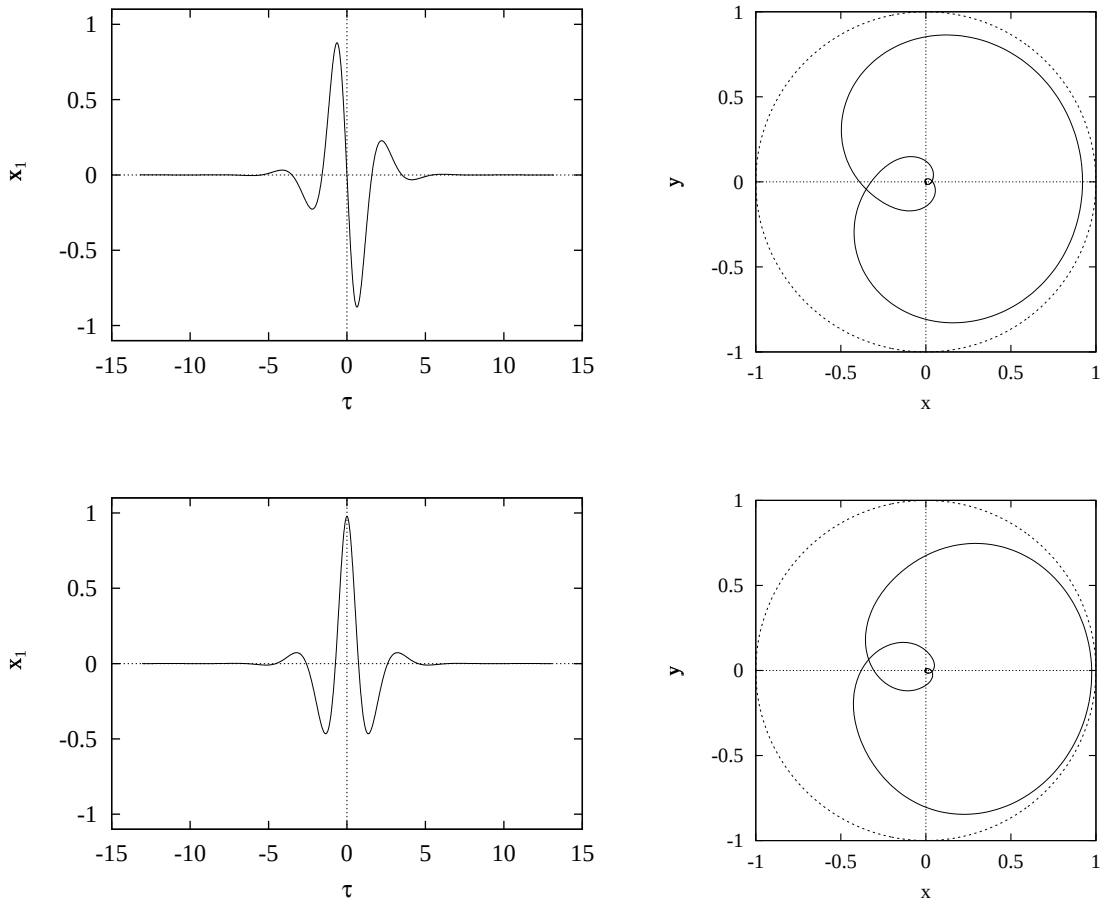

Figure 4: R_1-reversible (top) and R_2-reversible (bottom) primary homoclinic orbits (left) and the corresponding projections of the orbit of the top's centre of mass (right). The dotted unit circle represents the 'horizon' where the top goes through the horizontal plane through the pivot. ($\omega_0 = 3,\ \rho = 0.2,\ i_2/i_3 = 6/5$.)

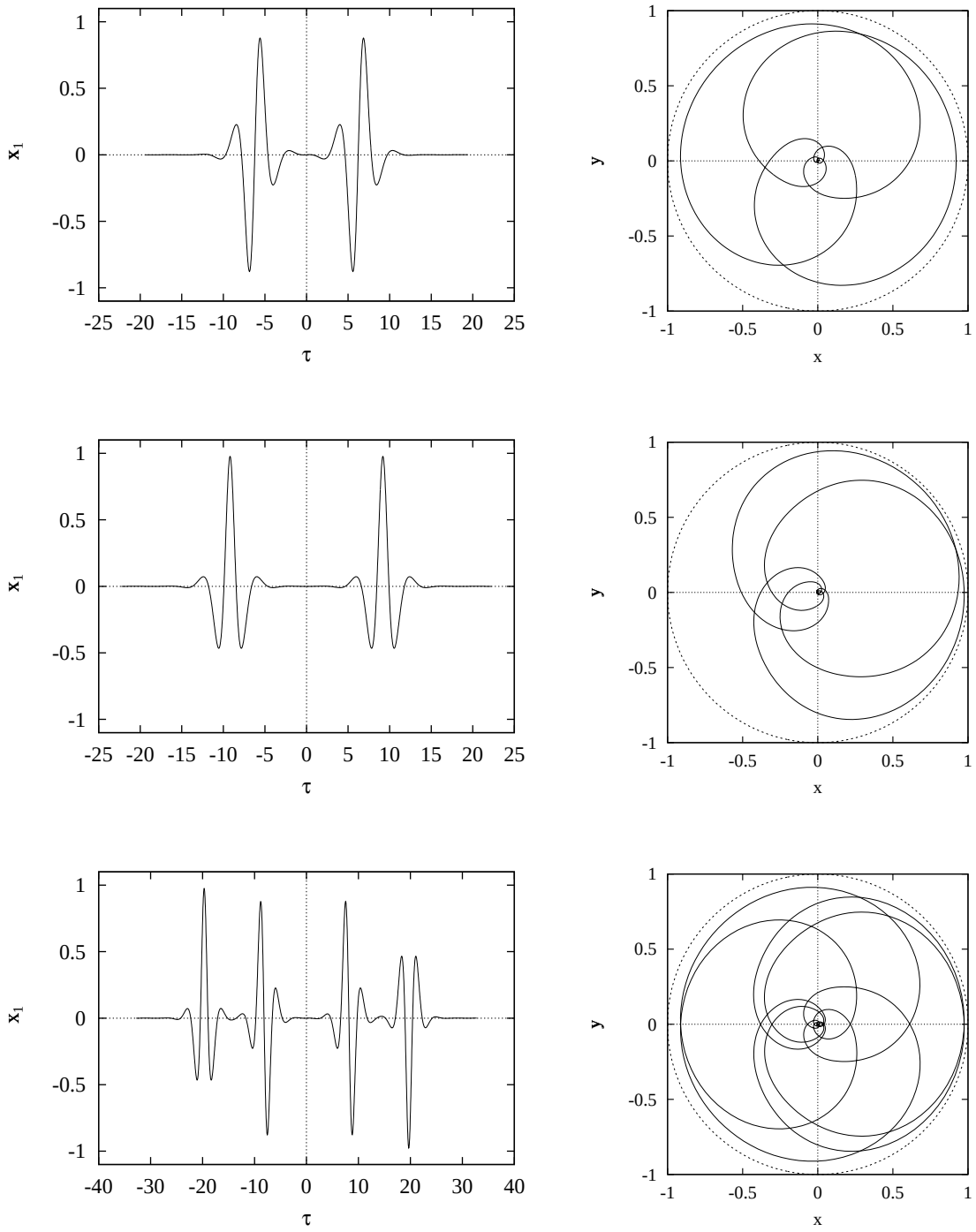

Figure 5: Multi-pulse homoclinic orbits: (top) R_1-reversible 2-pulse homoclinic orbit, (middle) R_2-reversible 2-pulse homoclinic orbit, (bottom) R_1-reversible 4-pulse homoclinic orbit. On the right are shown the corresponding projections of the orbit of the top's centre of mass. The dotted unit circle represents the 'horizon' where the top goes through the horizontal plane through the pivot. ($\omega_0 = 3,\ \rho = 0.2,\ i_2/i_3 = 6/5$.)

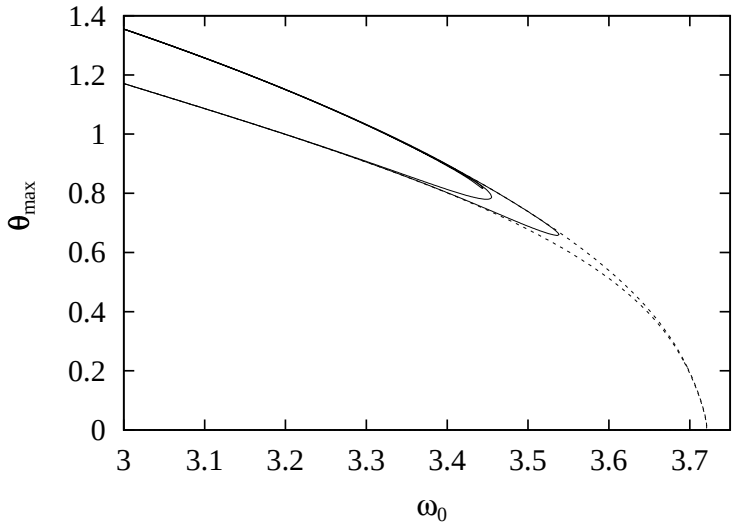

Figure 6: Continuation results for homoclinic orbits at $\rho = 0.2$. The dotted curves are for the two primary orbits of Fig. 4, the lower one being for the R_1-reversible solution. The solid curves are for the multi-pulse orbits of Fig. 5. Only the primary orbits bifurcate (at $\omega_0 = 3.721038$); the multi-pulse orbits form limit points. The R_2-reversible 2-pulse reaches furthest down. The 4-pulse is barely visible and lies entirely near the upper primary branch. $\theta_{\max}$ is the maximum nutation angle, in radians, reached along an orbit.

addition, infinite families of multi-pulse homoclinic orbits and horseshoe-type chaos in that same region. With the shooting method mentioned above we were able to locate whole series of these multi-pulse homoclinic orbits some of which are depicted in Fig. 5. They essentially consist of any number and combination of the four primary solutions separated by any number of small oscillations. The small oscillations correspond to rotations of the top subtending a small solid angle about the upright state. The shooting method used exploits the reversible symmetry of the problem and hence only finds reversible solutions, but asymmetric solutions exist as well. Clearly, for reversible solutions there are constraints on the possible combinations of primary pulses and their separating oscillations.

The multi-pulse homoclinic orbits do not bifurcate at ω_{c2} in Fig. 2, but disappear pairwise in limit points as this line is approached. Multi-pulse orbits do however exist arbitrarily close to this line. The same is true when approaching the integrable limit at $\rho = 0$ (either from positive or negative ρ), where only primary homoclinic orbits exist. Some continuation results illustrating the above are given in Fig. 6. In this figure $\theta_{\max}$ is the maximum nutation angle reached along an orbit, i.e., the largest angle the top's axis falls away from the vertical when going through its homoclinic motion. More information on the complexity of the structure of homoclinic orbits in the problem can be found in [7].

The two R_2-reversible primary homoclinic orbits can be continued outside the region of complex eigenvalues into the region of real eigenvalues. Indeed, it was found in [8] that, due to symmetry, only the R_2-reversible primary homoclinic orbits bifurcate from the Hamiltonian pitchfork line ω_{c3}. This behaviour is recovered in the present system. (It should be noted, though, that the line ω_{c3}, which was important for rods, is unimportant for the stability of

tops.) In contrast, when an R_1-reversible solution is continued towards the line ω_{c1} then its single pulse splits into two pulses which run off in opposite directions, reaching infinity at ω_{c1} (see also [7]).

4 Discussion

By using results from homoclinic bifurcation theory we have argued that the equations of motion for a top that has its centre of mass on one of its principal axes, admit infinitely many (multi-pulse) homoclinic solutions. These solutions provide infinitely many ways for the slowly spinning upright top to fall down. The existence of these solutions has been verified numerically and a sample of them has been computed. The use of homoclinic toppling and recovery motions has been proposed as a fast and energy-efficient means of reorienting spinning bodies such as satellites by applying suitable control mechanisms making use of the geometric phase difference, i.e., the different orientation in space, between the initial and final state of the body [2] (see also [3]).

We have introduced the inertia triangle to indicate regions of different behaviour for tops of different shapes, and studied instability through a Hamiltonian-Hopf bifurcation in some detail. It has also been noted that tops with certain values for their inertias can be destabilised in a different way (by two of the eigenvalues becoming real), but we have not explored this scenario any further. The relevant normal form has recently been computed by Langbort [13], taking account of both reversing symmetries R_1 and R_2. It is concluded that for some set of ρ-values a *pair* of symmetric homoclinic orbits exist for parameters below the m_{c4} curve in Fig. 2, but also that for other ρ-values no such primary homoclinic orbits exist. Given this situation, the work of Mielke, Holmes & O'Reilly [17] becomes relevant. They showed the existence of horseshoe-type chaos, and again infinitely many n-pulse ($n > 1$) homoclinic orbits, near a saddle-centre (i.e., two real and two imaginary eigenvalues) in a general 4-dimensional reversible Hamiltonian system, provided a primary homoclinic orbit exists and a certain normal form sign condition is satisfied. A further analysis of this possibility falls outside the scope of this short paper.

We finally mention that in a real top damping and friction will prevent full recovery from the toppling motion back to the upright state. Also, in such a system the complex issues of dissipation induced instabilities arise. For more on this the reader is referred to [4, 15] and references therein.

Acknowledgments

The authors would like to thank C. Langbort and G. Iooss for making available their recent normal form calculations. Useful references from an anonymous referee are also much appreciated. GvdH is supported by a Royal Society Research Fellowship.

References

[1] S.S. Antman, *Nonlinear problems of elasticity* (Springer-Verlag, Berlin, 1995).

[2] A.M. Bloch, J.E. Marsden, Control and stabilization of systems with homoclinic orbits, *Proc. of the 27th IEEE Conf. on Decision and Control IEEE, New York*, 2238-2242 (1989).

[3] A.M. Bloch, P.S. Krishnaprasad, J.E. Marsden, G. Sánchez de Alvarez, Stabilization of rigid body dynamics by internal and external torques, *Automatica* 28, 745-756 (1992).

[4] A.M. Bloch, P.S. Krishnaprasad, J.E. Marsden, T.S. Ratiu, Dissipation induced instabilities, *Ann. Inst. Henri Poincaré* 11, 37-90 (1994).

[5] R.L. Devaney, Homoclinic orbits in Hamiltonian systems, *J. Diff. Eqns.* 21, 431-438 (1976).

[6] H. Goldstein, *Classical mechanics*, 2nd ed. (Addison-Wesley, Reading, 1980).

[7] G.H.M. van der Heijden, A.R. Champneys, J.M.T. Thompson, The spatial complexity of localised buckling in rods with non-circular cross-section, *SIAM J. Appl. Math.* 59, 198-221 (1999).

[8] G.H.M. van der Heijden, J.M.T. Thompson, Lock-on to tape-like behaviour in the torsional buckling of anisotropic rods, *Physica D* 112, 201-224 (1998).

[9] R. Hill, Principles of Dynamics, Pergamon Press, Oxford, 1964.

[10] P.J. Holmes, J.E. Marsden, Horseshoes and Arnold diffusion for Hamiltonian systems on Lie groups, *Indiana U. Math. J.* 32, 273-310 (1983).

[11] G. Iooss, M.C. Pérouème, Perturbed homoclinic solutions in reversible 1:1 resonance vector fields, *J. Diff. Eqns.* 102, 62-88 (1993).

[12] S. Kehrbaum, J.H. Maddocks, Elastic rods, rigid bodies, quaternions and the last quadrature, *Phil. Trans. R. Soc. Lond. A* 355, 2117-2136 (1997).

[13] C. Langbort, Normal form for the saddle-centre bifurcation in the twisted rod problem, technical note, INLN, Nice (2000).

[14] J.H. Maddocks, On the stability of relative equilibria, *IMA J. Appl. Math.* 46, 71-99 (1991). A discussion of the eigenvalue behaviour at relative equilibria of the asymmetric top does not actually appear in this published version but in an unpublished addition to Section 7 of the paper.

[15] J.H. Maddocks, M.L. Overton, Stability theory for dissipatively perturbed Hamiltonian systems, *Comm. Pure and Applied Math.* 48, 583-610 (1995)

[16] A. Mielke, P. Holmes, Spatially complex equilibria of buckled rods, *Arch. Rat. Mech. Anal.* 101, 319-348 (1988).

[17] A. Mielke, P. Holmes, O. O'Reilly, Cascades of homoclinic orbits to, and chaos near, a Hamiltonian saddle-center, *J. Dyn. Diff. Eq.* 4, 95-126 (1992).